Report on Measurement of Stray Fields

28.02.2013

Abstract

Date of measurement: 28.02.2013. People present at measurement: O.Grover, J. Kocman, T. Markovic (author of this report), V. Svoboda, J. Stockel. Measurement/estimation of stray fields of tokamak GOLEM chamber and comparison to models.

1 Motivation and structure

This report contains results obtained from measurement of tokamak GOLEM chamber stray fields. These fields are expected (and measured) to be of vertical direction and have influence on plasma breakdown. Their quantification is motivated by study of breakdown induced by newly installed ECR heating on tokamak GOLEM.

Structure of report: Section 2 describes experimental arrangement and data processing methods, then presents results of the measurement and their discussion. Section 3 describes three different models of tokamak chamber magnetic field and compares results from previous section to their output. Section 4 presents model of particle trajectory in GOLEM pre-breakdown magnetic field and shows how length of magnetic field line can be obtained. Last section 5 summarizes the report and presents author's suggestions for future investigations.

2 Measurement Section

2.1 Experimental Arrangement and Data Analysis Method

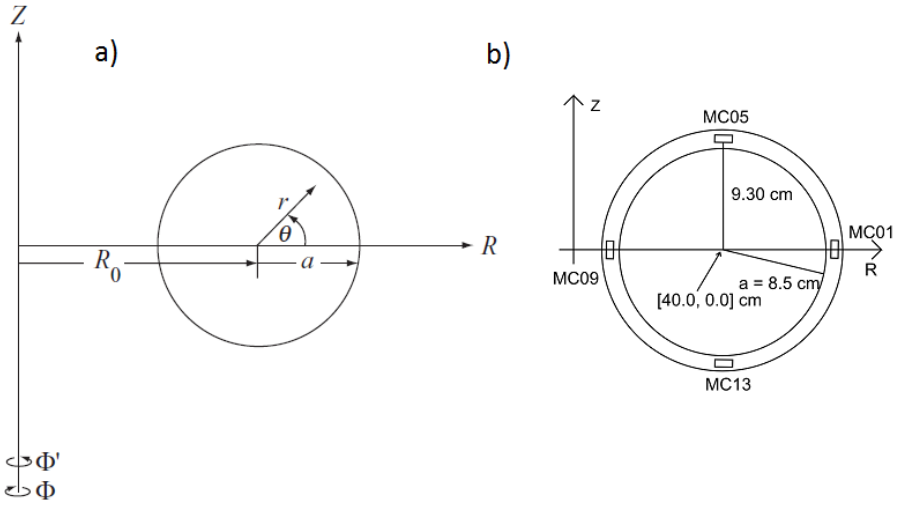

Figure 1: a) coordinate system of report. b) location and nomenclature of Mirnov coils.

For coordinate system of the whole report, see fig. 1a. On tokamak GOLEM, toroidal magnetic field B_T is of ϕ' direction and intensity of electric toroidal field E_T is of ϕ direction. Since E_T is responsible for plasma (and chamber) current drive, magnetic field and plasma current are anti-parallel in this tokamak. During plasma existence, total chamber current I_{tot} is negligible – not only relatively to plasma current I_{plasma}, but also to value of I_{tot} during vacuum discharge (i.e. discharge without plasma). This is because plasma with its low resistivity represents major conductor in such system.

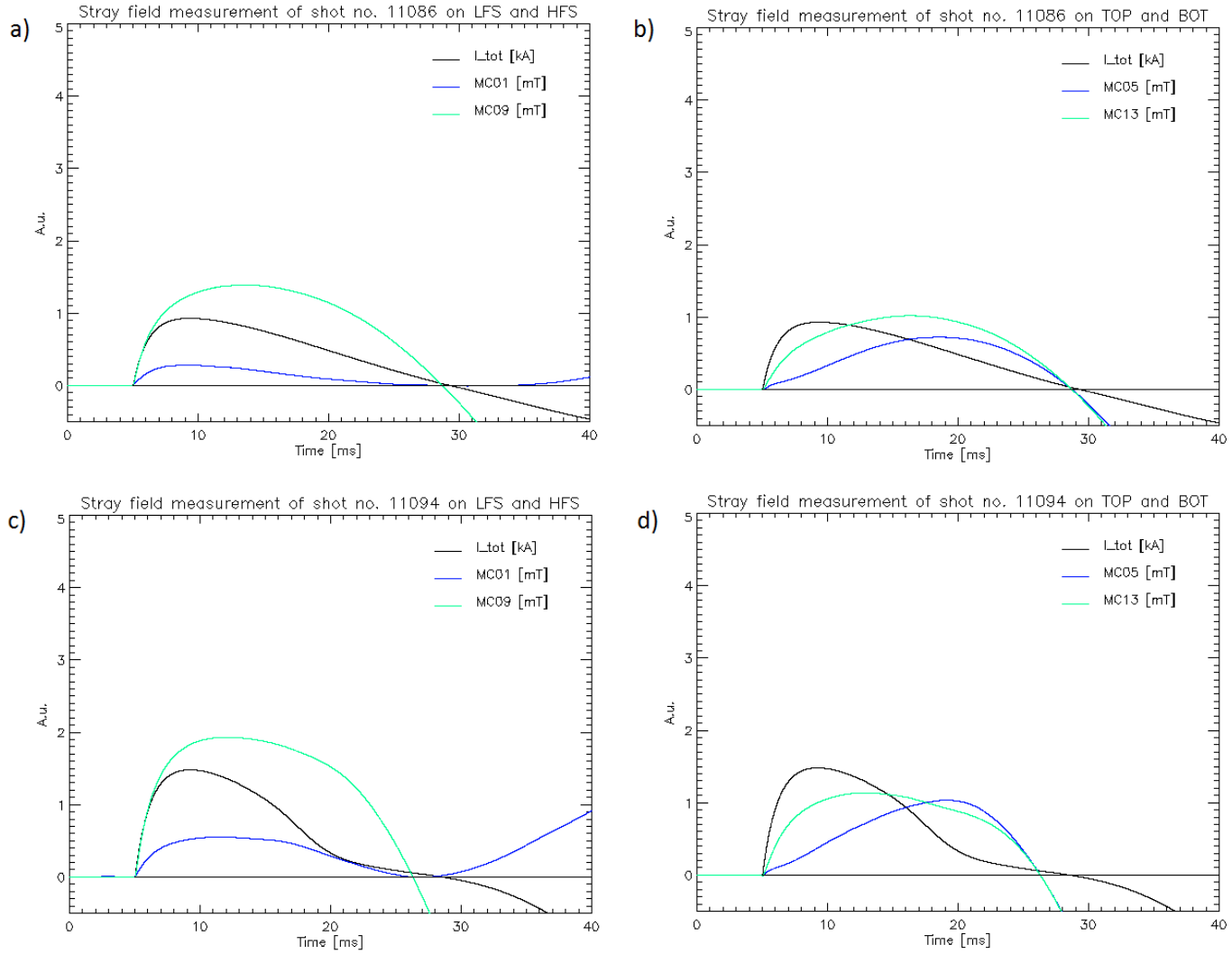

Figure 2: Measured stray fields. Directions were modified to be positive in plots. Vertical field is pointed DOWNWARDS, horizontal field is pointed OUTWARDS from torus major axis. For location of coils, see fig. 1b. a) Vertical B_s component with unsaturated core. b) Horizontal B_s component with unsaturated core. c) Vertical B_s component with saturated core (see I_{tot} evolution change). b) Horizontal B_s component with saturated core.

Nonetheless, without plasma can I_{tot} reach up to 2 kA, which would imply induction of additional non-negligible magnetic field. This field was measured during dedicated experimental session. Effect was clearly visible in data of shots no. 11082, 11083, 11084, 11085, 11086, 11087, 11089, 11091, 11094 and 11095, with different degrees of iron core saturation and I_{tot} values. Detection sensors in this session are represented by set of 4 old Mirnov coils for local B measurement (see fig. 1b), by Rogowski coil for I_{tot} measurement and by poloidal flux loop sensor for U_{loop} measurement. New rack of 16 MHD activity coils was used as well, however data from these were far less conclusive as those from old 4-rack. Since detection loops are based on Faraday's law of induction, coils detect only component of B normal to their effective area $A_{eff} = 37$ cm^2:

$$B(t) = \frac{1}{A_{eff}} \int_0^t U(\tau) \mathrm{d}\tau,$$

where $U(t)$ is voltage on the ends of coil in time (not necessary the same as that on the ends of data-acquisition cables leading to coil) and $\mathrm{d}\tau$ is sampling time period ($f_{sample} = 1$ MHz). This principle is disadvantageous for numerical integration (i.e. where sum is not provided by electrical circuit, but by manual sumation of detected U signal), since errors, drifts and effect of transient events add to each other and influence the whole signal (not only during the part of signal when they took place). DC offset voltage of signal is straightforward to correct for by using signal before current drive start. The main difficulties in data interpretation were casued by drifts and transient events present after start of current drive, since there it is not simple do distinguish drifts from actual experimental data. Therefore, following assumption was made:

In the whole session, the only magnetic field in the whole tokamak was the one trapped inside of iron core and stray field

	LFS	HFS	TOP	BOT
B_Z [mT/kA]	-0.38 ± 0.08	-1.3 ± 0.1	–	–
B_R [mT/kA]	–	–	0.72 ± 0.07	0.8 ± 0.2

Table 1: Measurements of B_s density over the whole session, with positive directions as shown in fig. 1. Void values mean that there were no corresponding sensors present on that location.

from total chamber current I_{tot}. I_{tot} varies in time according to rate of change of magnetic flux in transformer core (see 3 for details), going from 0 to max and then through 0 to negative values, as damped oscillation of RLC system of primary winding dictates. Inductance of chamber is neglected in this report, therefore in time t_0 where $U_{loop}(t_0) = 0$ (i.e. when chamber current driving $E_T = 0$), stray field $B_s(t_0) = 0$ as well, yielding $B_{det}(t_0) = 0$ on sensors. It was then assumed that all the other errors in signal take form of DC offset, constant in time, which emerges in the moment of current drive switch. Using $B_{det}(t_0) = 0$ constraint as reference point, correction across the whole signal was made. Results of that are provided in fig. 2. The analyzed quantity is density of stray magnetic field B_s per I_{tot}, i.e. $\frac{\max(B_s)}{\max(I_{tot})}$ [mT/kA].

2.2 Results and discussion

Fig. 2 represents typical data obtained by methods described above. On LFS and HFS, B_s vertical component of stray field is **downwards**, while on TOP and BOT is horizontal component of stray field **outwards** from major axis of torus. More general result, obtained over the whole session is stated in tab. 1. It can be seen that B_s density does not fluctuate much with change in global parameters, i.e. does not depend on value of I_{tot}, as long as iron is in linear response region. When iron is close to saturation however, measured B_s changes its character of time evolution. This might be due to iron stray fields (not the ones by chamber) – magnetic flux of current drive that escaped saturated iron. This issue is open for future analysis, but it is not much relevant for breakdown magnetic field studies (i.e. for scope of this report).

3 Chamber Models

3.1 Homogeneous Current Model

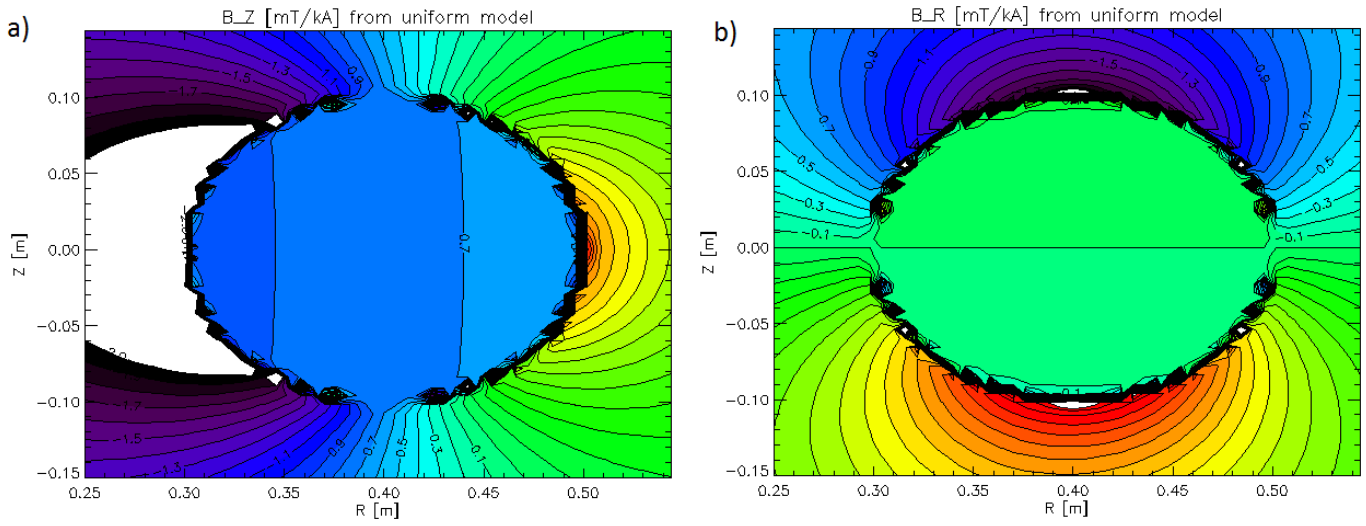

Figure 3: Components of B_s density using homogeneous current model. Coordinates explained in fig. 1. a) represents B_Z component and b) B_R component.

Model of stray fields is necessary in order to obtain both of B_s component in all the locations of future interest and not to be bound only to locations where measurement took place in past. The **homogeneous current model** assumes that I_{tot} density is uniform across chamber. I.e. if chamber is divided among N independent loops of poloidal coordinates (R_i, Z_i), uniformly distributed along chamber cross section, then their currents $I_i = I_{tot}/N$. Fig. 3a describes B_Z density from such model, while 3b gives B_R density.

3.2 Simple Inductive Model

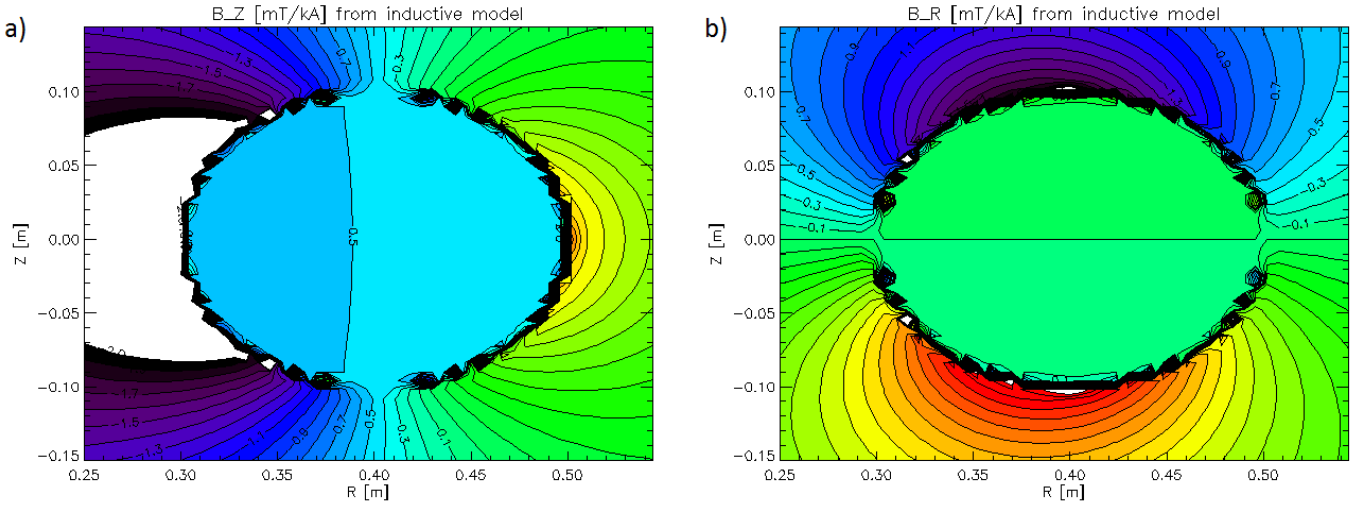

Figure 4: Components of B_s density using inductive model. Coordinates explained in fig. 1. a) represents B_Z component and b) B_R component.

Uniform current distribution across chamber would require unreallistic E_T profiles, therefore next model exploits the knowledge of E_T profile for tokamak vaccum field. Rate of change of magnetic flux thorough central column yields:

$$-\frac{\partial}{\partial t}\int_{S_l}\mathbf{B}\cdot\mathrm{d}\mathbf{S}=\oint_l\mathbf{E}\cdot\mathrm{d}\mathbf{l}:=U_{loop}.$$

Since $\mathbf{B}$ of current drive is present exclusively inside of iron core, any closed contour l will yield the same U_{loop} as long as central column is encircled. Therefore:

$$U_{loop}(R,Z)=\text{const}\quad\text{and}\quad E_T\sim\frac{1}{R}.$$

If chamber is once again considered as set of N independent loops with zero inductance (i.e. are fully characterized by resistivity per unit of length ρ_l) and of currents I_i, then:

$$I_i(R_i)=\frac{U_{loop}}{2\pi\rho_l R_i}\sim\frac{1}{R_i},$$

unlike the previous model. Using constraint $I_{tot}=\sum_i I_i$ then yields more practical relation:

$$I_i=\frac{1}{R_i}\frac{I_{tot}}{\sum_j 1/R_j}. \tag{1}$$

Fig. 4 shows respective B_s density profiles according to this model.

3.3 Simple Inductive Model With Tokamak Core

Unsaturated ferromagnetic core naturally influences magnetic fields in their vicinity. Precise explanation is beyond scope of this report. The main physical priniple is that any current in vicnity of core is screened by currents induced along boundary of this core. Screening currents naturally induce magnetic field and thus change in magnetic topology occurs. This effect diminishes with distance of screened current from core, as well as with saturation of core. The latter is safely assumed not to take place in before breakdown (thought core may be saturated after the discharge). In this specific case, the screened currents were those of chamber, calculated by eq. 1 (i.e. this is modification of previous model). Results are presented in fig. 5.

3.4 Comparison of Models to Each Other and to Measured Data

It is evident on first sight in figs. 3,4,5, that predicted stray field gets weaker with every correction. Comparison of all the models to measured data in fig. 6 yields, that for magnitudes of B_s densities measured on HFS, no plausible explanation

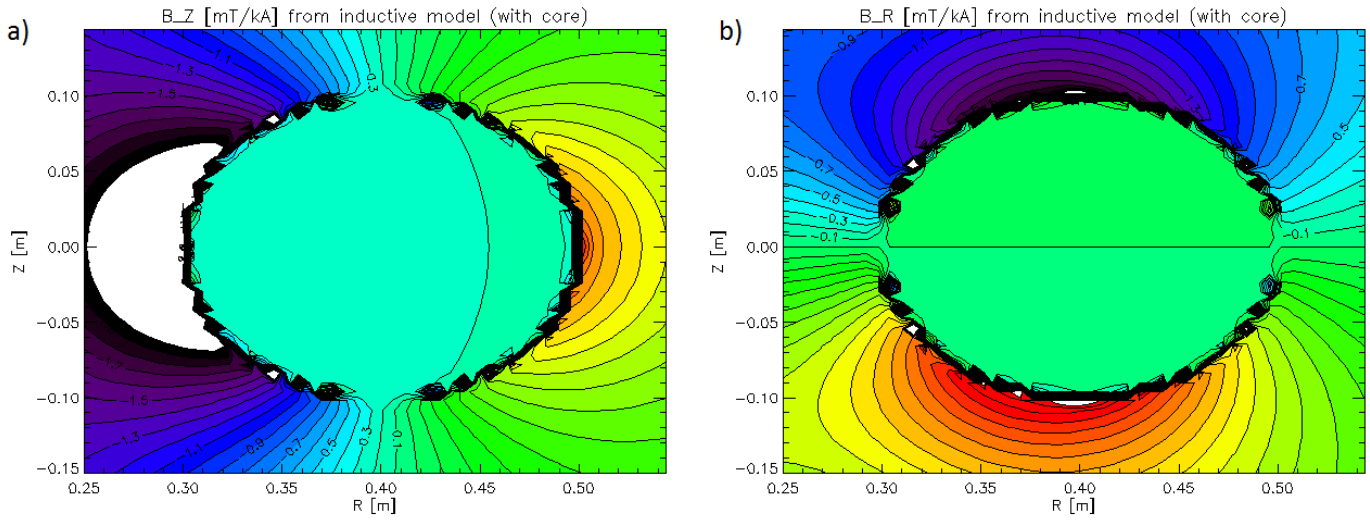

Figure 5: Components of B_s density using inductive model + iron core model. Coordinates explained in fig. 1. a) represents B_Z component and b) B_R component.

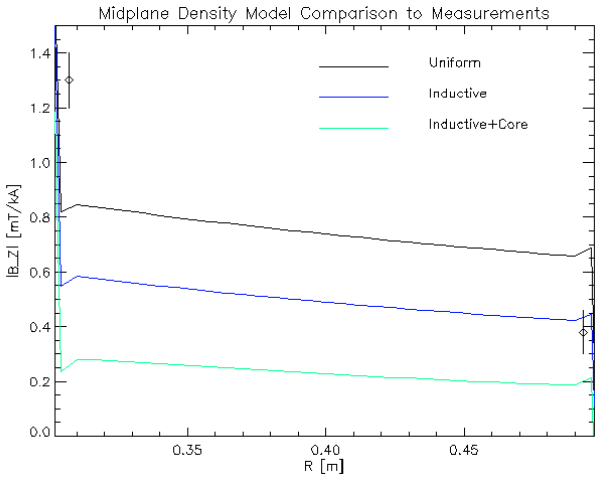

Figure 6: Comparison of measured values (rhombs with errorbars) to different models presented in section 3. Plot shows midplane, i.e. at $Z = 0$ coordinates.

was found. A slightly better is situation on LFS, where inductive model without iron core prediction falls into uncertainty interval of measured values. However, all the models predict that B_R in TOP and BOT is very close to 0, which is in strong contrast to measured values (see tab. 1).

4 Charged Particle Trajectories in GOLEM Fields

4.1 Trajectory of Particle

Usefullness of B_s model lies mainly in possibiility of prediction of trajectory of charged particles in vacuum field before breakdown. Trerefore, numerical model of particle trajectory in tokamak GOLEM vacuum field was written, with particle trajectory being specified using Boris-Bunemann numerical method of 4th degree of precision. Particle collisions with neutral gas are neglected, magnetic field is assumed to be sum of primary confinement toroidal field and vertical stray field, calculated by inductive model (the one without iron core).As for electric field, $E_T \sim 1/R$ field, magnitude given by U_{loop}. See caption in fig. 7 for parameter values of fields. Fig. 7a shows how B_s field induced by $I_{tot} \approx 1$ kA causes downwards macroscopic motion of electron that folows magnetic field lines while being accelerated by E_T. For electron of initial $v_{par}(t = 0) = 0$, it took 0.011 ms until it got from center of chamber to its bottom by acceleration from E_T and following $\mathbf{B_T} + \mathbf{B_s}$ field.

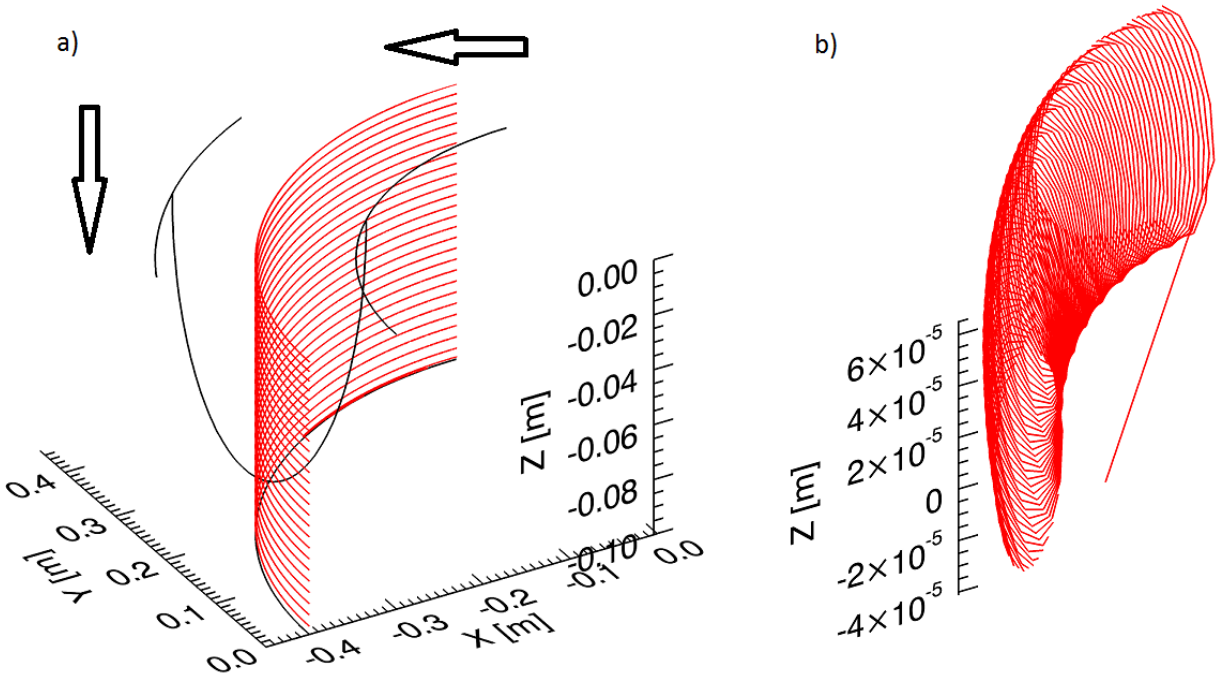

Figure 7: Trajectory of electron in GOLEM electro-magnetic fields. $B_T(R_0) = 0.4$ T, $U_{loop} = 15$ V, electron initial position in $(R, Z) = (0.4, 0.0)$, $v_{par}(t = 0) = 0$. a) shows macroscopic movement, with arrows representing direction of particle movement. Detail in b) shows Larmor gyration around field lines.

4.2 Field Line Length

Simulations of particle trajectory thus imply that it mainly follows magnetic field line, while effects of drifts arising from Larmor gyration of particle are negligible in comparison to this parallel motion. Therefore, magnetic field line length L_f might play major role in determination whether breakdown will occur or not. For the needs of further analysis, simple semi-analytical model of L_f was developed.

Let there be charged particle in chamber on poloidal coordinates (R, Z). Model from previous subsection (see fig. 7) shows that such particle will follow magnetic field line in toroidal direction, slowly drifting downwards until it will hit limiter. Let us make ansatz, that:

$$L_f(R, Z, B_{T_{cen}}, U_{loop}) = L_0(R, Z) + G(R, Z)\frac{B_{T_{cen}}}{U_{loop}}, \quad \text{where} \quad L_0(R, Z) = Z + \sqrt{a^2 - (R - R_0)^2}. \tag{2}$$

L_0 represents minimal trajectory of particle at $B_T = 0$ or $U_{loop} \to \infty$ – the particle will head straight down from its initial position (see fig. 1 for explanation of a and R_0). $B_{T_{cen}} = B_T(R_0)$, and $G(R, Z)$ is unknown function, dependent only on initial particle coordinates. This function can be obtained from results of L_f simulation with input parameters of R, Z, $B_{T_{cen}}$ and U_{loop} in following manner:

$$G(R, Z) = (L_f - L_0)\frac{U_{loop}}{B_{T_{cen}}}.$$

Evolution of this function across midplane (i.e. represents average L_f for field lines at given R) is shown in fig. 8a. Source data of the plot are available – upon request, on GOLEM wiki or in attachement to mail that contained this report.

Using G, it is possible to investigate validity of ansatz in eq. 2 – G obtained from previous relation for given (R, Z) should be constant across scan of $B_{T_{cen}}$ or U_{loop} if the ansatz is correct. Thus let G_{ref} be value of this function for U_{loop} and $B_{T_{cen}}$ in the middle of scanned intervals. If eq. 2 is fully valid, then $\frac{G}{G_{ref}} - 1 = 0$ for every U_{loop} and $B_{T_{cen}}$. Fig. 8b shows, that this is indeed the case for $R = R_0$. However, when approaching LFS, difference between G and G_{ref} can reach up to 10 % for very high values of B_T (see fig. 8c). On HFS, this difference can even reach 20 % (see fig. 8d) at high values of central field. Nonetheless, for standard pre-breakdown parameters, the difference stays on reasonably good tolerance levels.

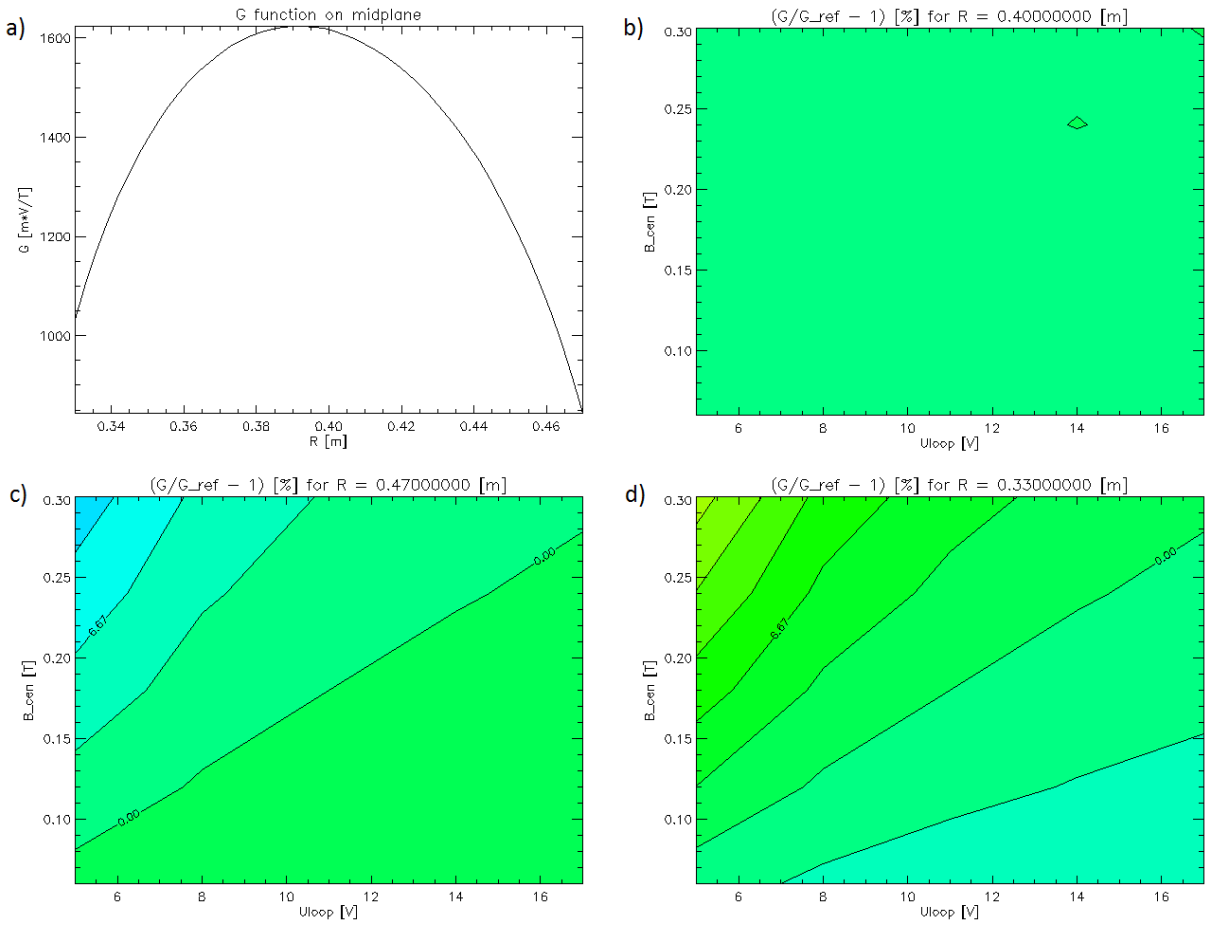

Figure 8: a) $G(R,0)$ function for eq. 2. This dependece was calculated using $U_{loop} = 12$ V and $B_T(R_0) = 0.17$ T. b), c) and d) – reliability of eq. 2 at different R (for $Z = 0$). Each level is 3.33 % high.

5 Discussion and Suggestions

Comparison of measurements to model calculations from section 3 yields substantial discrepancy. The more physically correct model is thought to be, the lesser stray field is expected. However, measurements on the other hand show that even the most overshot model is still far below the experimental value levels (at least on TOP, BOT, and HFS). This would imply that either measurement and data analysis method is wrong, or that models are insufficient.

As far as measurement method is concerned, there are several issues. By looking on character of data curves in fig. 2, it seems that time t_0 where $U_{loop}(t_0) = 0$ is improtant point of reference only for LFS probe curve. The other of data lines show no change in time derivation in vicinity of this point whatsoever (i.e. $\frac{\partial^2 B_{det}}{\partial t}(t_0) \approx 0$). Additionally, it is only LFS curve that seem to follow character of I_{tot} evolution. This would leave MC01 to be the most (if not the only one) reliable among the used sensors. Incidentally, it is this probe which corresponds to models the best. On the other hand, even if the behavior of the rest of the probes may seem suspicious, tab. 1 shows that their B_s densities do not depend much fluctuate on maximal I_tot in given experimental shot and thus implies that there indeed is magnetic field of much stronger magnitude than anticipated (at least on TOP and BOT). This points towards an additional physical effect which was not implemented into models in sec. 3. Since the sensors are placed in the vicinity of ports (except for MC09, which is on HFS), the best candidate for strong TOP and BOT field explanation might be distortion of current profile due to port presence. As for HFS probe, there is still possibility that B_s magnitude detected there might drop to modelled level, once better quality data (or better analysis method) are obtained (or not).

From the viewpoint of author of this report, it would be best to use MSL 3D Hall probe to measure and analyze stray fields in the same manner as it was done with Mirnov coils. This would enable to obtain the complete R profile across midplane, with probe being far from the ports and enable to detect both components of B_s at the same time. Also, principle of Hall sensros is different from inductive character of Mirnov coils and much more robust data can be obtained. Before any further analysis, more reliable data should be obtained and analyzed.

Once reliable measurements of B_s are obtained for chosen (R, Z) coordinates, it will be possible to seek the most

appropriate model for obtaining B_s in any location in vacuum vessel. That in turn will enable to obtain realistic values of field line length L_f by using eq. 2 (G however depends on used model of chamber, so it will be necessary to be recalculated first). Afterwards, investigation of relation of L_f quantity to plasma breakdown conditions may begin.